Received: 5 February 2024 | Revised: 1 April 2024 | Accepted: 3 April 2024

DOI: 10.1002/cem.3552

SHORT COMMUNICATION

Journal of CHEMOMETRICS WILEY

A short note on deep contextual spatial and spectral information fusion for hyperspectral image processing: Case of pork belly properties prediction

Puneet Mishra[1] | **Michela Albano-Gaglio**[2] | **Maria Font-i-Furnols**[2]

[1]Food and Biobased Research, Wageningen University and Research, Wageningen, The Netherlands

[2]IRTA-Food Quality and Technology & Finca Camps i Armet, Monells, Spain

Correspondence
Puneet Mishra, Food and Biobased Research, Wageningen University and Research, Wageningen, The Netherlands.
Email: puneet.mishra@wur.nl

Abstract

This study demonstrates a new approach to process hyperspectral images where both the contextual spatial information as well as the spectral information are used to predict sample properties. The deep contextual spatial information is extracted using the deep feature extraction from pretrained resnet-18 deep learning architecture, while the spectral information was readily available as the average pixel values. To fuse the information in a complementary way, a multiblock modeling approach called sequential orthogonalized partial least squares was used. The sequential model guarantees that the information learned is complementary from spatial and spectral domains. The potential of the approach is demonstrated to predict several physical and chemical properties in pork bellies.

KEYWORDS

artificial intelligence, data fusion, multivariate, spectroscopy, transfer learning

1 | INTRODUCTION

Hyperspectral imaging (HSI) is a novel spectroscopy technique that allows the exploration of spatially resolved spectral properties of materials in a nondestructive and noncontact manner.[1] The technique requires minimal sample preparation and can access surface properties of materials.[2] In some cases, information can be accessed up to a certain depth from the top layer.[3,4] For example, in the case of fresh fruit, the technique allows capturing information below the fruit skin.[5] HSI can be performed in various modalities depending on the light source and camera optics, such as fluorescence,[6] ultraviolet,[7] visible and near-infrared (VNIR),[3] shortwave infrared,[8] and Raman.[9] The application of HSI can be found in different domains of sciences, ranging from field applications for agricultural purposes to high-end pharmaceutical manufacturing.[10]

HSI in the VNIR range is the most commonly used spectral range for food and bio-process analysis.[1] One of the main reasons for this is that illumination and optical camera systems are readily available for the VNIR domain and can be easily integrated to run experiments. In some cases, fully standalone systems for HSI are also available.[11] For the application of interest in this study, that is, meat, VNIR HSI has been widely applied for the analysis of various types of meat such as chicken,[12] beef,[13] pork,[14] as well as seafood such as shrimps[15] and salmons.[16]

One of the main steps in using HSI in the spectral range of VNIR is that, for predictive modeling, calibrations need to be developed.[17,18] Calibrations are nothing but predictive models based on reference samples covering a wide variation in physicochemical properties of interest.[19] In the case of VNIR spectral modeling, some special chemometric methods such as partial least squares (PLS) are considered as the gold standard.[18] PLS allows handling the high multicollinearity in the VNIR data by projecting the data in the directions of maximum covariance.[20] PLS also performs data compression simultaneously, allowing the later development of multilinear models efficiently. For predictive modeling purposes, it is a common practice to extract the mean spectra of objects and then train the models with some ground truth data.[21]

In the domain of close-range HSI, several approaches have emerged to analyze the HSI data; however, most of them are limited to only using spectral information.[3,21] In fact, it can be observed that HSI in the close range is minimally treated as imaging but more as a point spectrometer capable of measuring spectra from different locations. The rich contextual spatial information available in the imaging domain of HSI is minimally used,[17] and also, minimal attention is paid to it during modeling. In some recent studies, the authors have started focusing on using spatial information for improved model building[22,23] as well as the validation of models in terms of spatial homogeneity/heterogeneity.[24] In recent studies,[22,23] the use of spatial information was supported by manually extracting spatial features such as grey level co-occurrence matrices from the pseudo-color images available from spectral images. Such studies have already shown that a combination of spatial and spectral information leads to improved model performance. However, such manual extraction approaches are limited by the number of filters that can be manually tuned and applied. On the other hand, deep learning (DL) has emerged as a potential tool to model imaging data.[25] The main benefit of DL models for image processing is that they allow automatic tuning and extraction of relevant features with multilayer neural networks depending on convolution operations. DL models for computer vision applications are trained on millions of images and carry the tendency to capture features applicable to generic image processing. Usually, for new applications, the models need not be trained from scratch but only fine-tuned to match the application.[26] This concept of fine-tuning is called transfer learning and has been described in a recent chemometric article.[27] Apart from transfer learning, the deep pretrained models can also be used to perform sole feature extraction.[28,29] This can be performed by removing the output layer of the deep models and using the processed information until the second last layer as a feature vector, as proposed in this work and described later in the method section.

Similar to VNIR spectral data, the features extracted by DL models carry high multicollinearity as there are no specific constraints in the deep models to keep the features orthogonal. High multicollinearity indicates that PLS approaches[20] can still benefit in further polishing the deep features before they are combined with spectral information to build the final models. Also, the scale of deep features is totally different compared with the scale of the spectral data. In that regard, an optimal approach to fuse the deep features with the spectral information is to use chemometric multiblock approaches[30] such as sequential orthogonalized PLS regression.[31] In SO-PLS, only complementary information from data coming from different sources is extracted. In the presented case, this means only unique information from the spatial and spectral domain will be learned by the model for data compression and later for model development. This also means that the model will only accept information fusion if there is truly complementary information in the spatial and spectral domain. Some recent applications of SO-PLS for fusing information for hyperspectral analysis include fusion of data from hyperspectral images of different spectral cameras.[32,33]

The objective of this study is to present the potential of a new HSI processing strategy that combines the concept of spatial and spectral information fusion with deep feature extraction. The study aims to use the freely available deep network resnet-18 for feature extraction from the spatial domain of HSI and then combine that with the spectral information in a multiblock framework of sequential modeling. The application of the methodology is demonstrated on a real case of VNIR HSI-based pork belly analysis to predict several physicochemical parameters.

2 | MATERIALS AND METHOD

2.1 | Sample, HSI, and reference analysis

A total of 182 bellies from the left half of carcasses were randomly selected 24 h postmortem from various commercial slaughterhouses, ensuring a wide variability in genotypes and sexes. The bellies were obtained using anatomical points of reference before being deboned. Subsequently, the bellies were deboned, weighed, and the belly weight proportional to the carcass weight was calculated as a percentage (referred to as belly proportion). In this study, three distinct

chemical parameters (fats, proteins, and iodine value) and two physical parameters (flop angle and finger pressure test) were measured and utilized for predictive modeling.

All samples were initially imaged with the HSI system, which consisted of a spectrograph, a camera, a conveying platform, and a computer supported with data acquisition software (Spectronon, Resonon Inc., Bozeman, MT, USA). The conveying platform was positioned 50 cm away from the camera lens and was driven by a stepping motor at a speed of 0.03 m/s. Four 50 W tungsten-halogen lamps were strategically placed to illuminate the camera's field of view. In this push-broom HSI system, spectral images were collected line by line in reflectance mode within the wavelength range of 386–1015 nm, with 300 wavebands at 2 nm intervals in the spectral domain. The HSI system underwent calibration before each imaging session: A dark image (0 % reflectance) was obtained by covering the camera lens with its opaque cap in the absence of light, and a white image was captured using an 8 × 20 cm Teflon piece (99.9% reflectance). To extract spectral information for each belly, the image underwent segmentation, and all pixels corresponding to fat were averaged to generate a mean spectral profile for each belly.

For protein content, the belly (without skin and bones) was homogeneously minced with a cutter, vacuum-packed, and frozen at −20°C for further analysis. Proteins (Kjeldahl nitrogen) were then analyzed from the minced belly following official methods.[34] Lipids from the minced bellies were extracted using chloroform/methanol (1:2, v/v) and quantified according to the method described in Bligh and Dyer.[35] After lipid extractions, fatty acid (FA) compositions of subcutaneous fat and minced belly samples were determined by acidic trans-esterification in the presence of sodium metal (0.1 N) and sulfuric acid (5% sulfuric acid in methanol).[36] The FA methyl esters (FAME) were analyzed by gas chromatography, using a Hewlett–Packard HP-4890 Series II gas chromatograph equipped with a split/splitless injector and a flame ionization detector (FID). Finally, individual FAME were identified by comparing their retention times with those of reference standard mixtures (Sigma Chemical Co., St. Louis, MO, USA). The iodine value (IV) of belly samples was determined according to the modified AOCS equation obtained by Fiego et al,[37] by including all the unsaturated FAs detected by gas chromatography.

As a physical characteristic, belly firmness was determined using the bar suspension method.[38] This involved employing a horizontal stainless-steel bar with a diameter of 20 mm, where the bellies were suspended skin side up and down on their central short axis. This arrangement allowed both the caudal and cranial ends to freely fall. The flop distance, which is the distance between the dorsal extremities, was measured, and the upper angle of the isosceles triangle formed was calculated using this flop distance and the length of the belly (referred to as the flop angle). After removing the skin 48 h postmortem, the fat firmness of the bellies was also measured by finger pressure (referred to as finger pressure) according to a predetermined scale as described by Soladoye et al.[39]: "(1) firm fat, no finger mark, no floppy; (2) firm fat, no finger mark, partly floppy; (3) soft fat, finger mark remains, floppy; (4) soft fat, finger mark remains, very floppy; (5) soft fat, finger mark remains, very floppy, oily". The finger pressure was assessed by two trained evaluators, and the average of the scores was used, with lower scores indicating greater firmness.

2.2 | Hyperspectral image analysis

The images were measured with blue background; hence, segmentation of the images was performed using a partial least squares discriminant analysis (PLSDA) model, distinguishing between the fat and nonfat parts in the imaged scene. The model was constructed using manually selected spectra from the image and subsequently optimized through a fivefold cross-validation analysis. This model was then applied to all the images to segment all the images and to extract mean spectra for all the belly samples. Using mean spectra, samples were partitioned into calibration and test set using the Kennard-Stone[40] algorithm. The same partition was used for modeling and calibration for all the response variables. Spectral data were preprocessed with variable sorting for normalization to eliminate physical effects from spectra.[41]

In this study, the resnet-18[42] model trained on over a million images was used as a pretrained network for deep spatial feature extraction. Deep models were used for feature extraction task by removing the final layer of the network and using the output of the second last layer of the network as the input to another model. In the presented case, the output of the second last layer carrying deep features was combined with the spectral information in the multiblock framework. In the case of resnet-18, the input spatial size is 224 × 224; hence, all the pseudo color images were reshaped to 224 × 224, before input to the network. The pseudo color images were constructed using bands 750, 670, and 500 as red, green, and blue. The extracted spatial features were 1-D vector of size 1 × 512; hence, for every image,

the deep network provided 512 features. The spatial data were also partitioned using the same partition. The spectra and spatial information were fused with the multiblock method called sequential orthgonalized PLS as explained in following section.

2.3 | Sequential PLS algorithm for information fusion

In following, a description of the sequential data fusion algorithm is provided, presenting the key mathematical steps in the algorithm. All matrices are denoted with bold uppercase typeface such as $\mathbf{X}$. All vectors are denoted with bold lowercase typeface such as $\mathbf{y}$. All scalars are denoted with italic typeface such as a. Define $\mathbf{y}$ $(n \times 1)$ as the response vector, $[\mathbf{X_{spatial}}, \mathbf{X_{Spectral}}]$ as a multiblock multivariate input where first block is the deep spatial information and second block are the spectral information. The spatial information is placed earlier than spectral because such information is easy to access with just RGB cameras while the spectral information is only available with spectrometers. Let A be the desired number of components to be extracted. Both the predictor and the response are assumed to be mean-centered. Note that in the following algorithm, the user needs to define the order of the component extraction, for example, out of A number of component, how many to be extracted from each block. For example, when the defined order involves selecting components first from the spatial data and later from the spectral data, the algorithm allows developing sequential model. In the cross-validation analysis (fivefold), different components extraction orders are explored to find the optimal components from each data block. To keep the algorithm to converge, the max number of components for each block was kept maximum to 20.

Algorithm for sequential partial least squares modeling

$for a = 1:A$	- loop over *A components to be extracted according to the defined component extraction order*
$\mathbf{w}_{\mathbf{o}_a} = \mathbf{X}_{\mathbf{o}_a}{}^t\mathbf{Y}$	- loading weights extracted from the data block as defined in component extraction order
$\mathbf{t}_a = \frac{\mathbf{X}_{\mathbf{o}_a}\mathbf{w}_{\mathbf{o}_a}}{\|\mathbf{X}_{\mathbf{o}_a}\mathbf{w}_{\mathbf{o}_a}\|}$	- estimate normalized score vector from the data block as defined in component extraction order
$\mathbf{q}_{\mathbf{o}_a} = \mathbf{y}^t\mathbf{t}_a$	- y loading′s
$\mathbf{y} \Leftarrow \mathbf{y} - \mathbf{t}_a\mathbf{q}_a^t$	- y deflation
$for i = 1:2$	- loop over spatial and spectral blocks to extract spatial and spectral specific loading′s
$\mathbf{p}_{i_a} = \mathbf{X}_{i_a}^t\mathbf{t}_a$	- Block specific X loading′s
$\mathbf{X}_{i_a} \Leftarrow \mathbf{X}_{i_a} - \mathbf{t}_a\mathbf{p}_{i_a}^t$	- Block specific deflation using extracted score
end	- accumulate loading weights (W), scores (T)and loading′s (P)in matrices (not shown)
end	- end of component loop
$\mathbf{R} = \mathbf{W}(\mathbf{P}^t\mathbf{W})^{-1}$	- projections for score prediction*
$\mathbf{B} = \text{cumsum}(\mathbf{RQ}^t)$	- regression coefficients
$\mathbf{B}_0 = \overline{\mathbf{Y}} - \overline{\mathbf{X}}\mathbf{B}$	- mean compensation

*Calculation of projection for score predictions **(R)** assumes spatial and spectral loading's and loading weights stacked with matrices of zeros for blocks not used for components extraction.

All model performances were evaluated using coefficient of determination, root mean squared error of prediction (RMSEP), and ratio of standard deviation of test set to the RMSEP. All analyses were carried out in MATLAB 2021b (Natick, MA, USA).

3 | RESULTS

The prediction results for iodine value, fat, and protein content are shown in Figures 1–3, respectively. The spatial information was able to predict all three chemical parameters with a good coefficient of determination ($r^2 > 0.55$). For low-cost applications, this indicates that a relatively well-performing imaging system can be developed with RGB cameras and DL. The model based on spectral information, carrying rich chemical band overtones information, predicted all the chemical properties with a higher coefficient of determination and lower prediction errors than the spatial

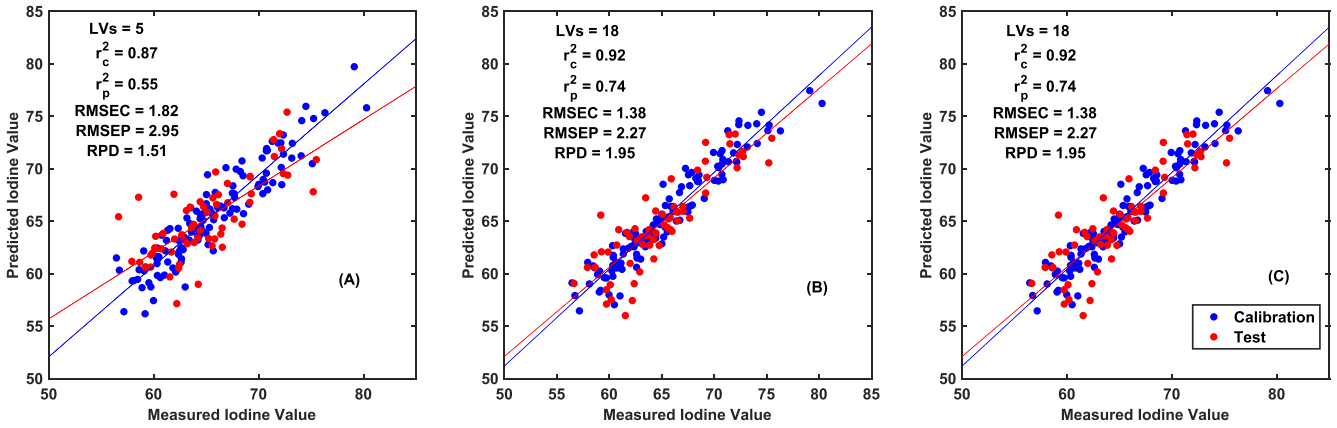

FIGURE 1 Iodine value prediction with (A) spatial information, (B) spectral information, and (C) sequential fusion model.

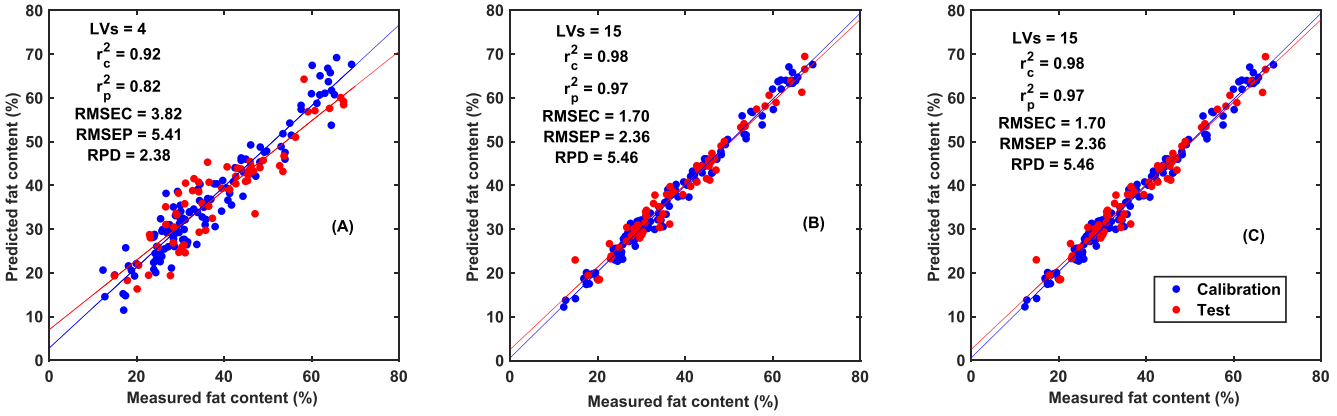

FIGURE 2 Fat content prediction with (A) spatial information, (B) spectral information, and (C) sequential fusion model.

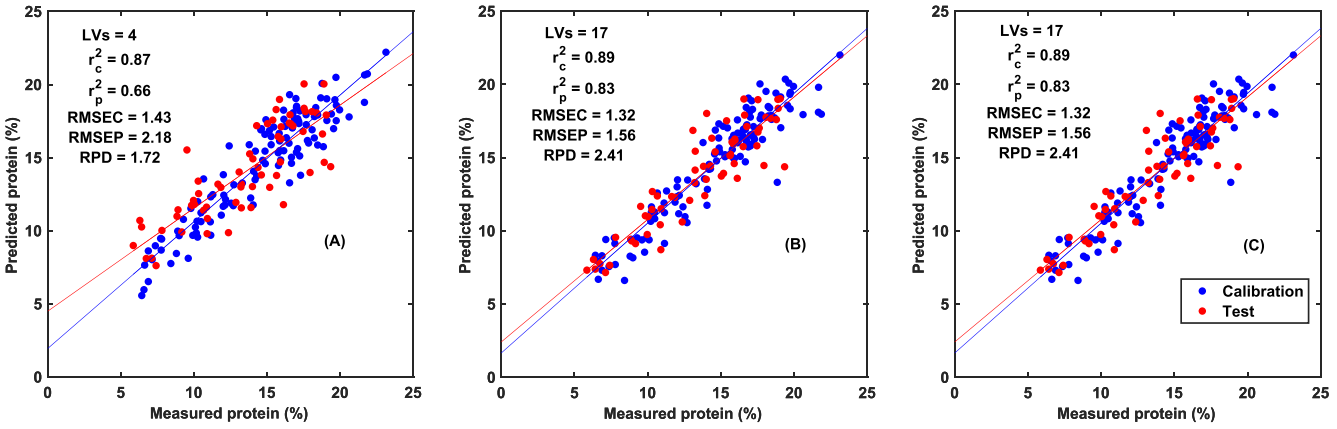

FIGURE 3 Protein content prediction with (A) spatial information, (B) spectral information, and (C) sequential fusion model.

information. The fusion of spatial and spectral information in the framework of SO-PLS found optimal models using only the information from the spectral domain. This is only possible if the information in the spatial domain related to chemical properties is already captured by the spectral information, as the SO-PLS model only models complementary information. For spatial information modeling, the optimal number of latent variables was almost three times less than the latent variables for spectral information. Overall, for chemical property prediction, the highest coefficient of

determination was obtained for fat content, followed by protein and then iodine value. For fat content and RPD of 5.46 was achieved with spectral information indicating that the model can be used for any application.[43] For protein content and iodine value, an RPD of 2.41 and 1.96 indicates that the model can only be used for rough screening purposes.[43] For sole spatial information, the RPD values were only relevant for fat content, while for protein and iodine, the RPD values were low to not recommended model for routine use.[43]

For predicting physical parameters such as angle flop (Figure 4 and finger press score (Figure 5), spatial information either performed better than the spectral information in terms of lower prediction errors or showed similar performance. However, the fusion of spatial and spectral information performed better than both the individual spatial and spectral information-based models. The fusion modeling for predicting angle flop learned eight latent variables from spatial information and one latent variable from the spectral domain. The RMSEP with fusion was 13.4°, which was lower than the individual models based on spatial and spectral information. For predicting finger press score as well, the fusion model was obtained with 16 latent variables from spatial and 2 latent variables from the spectral domain, leading to the lowest RMSEP of 0.27. As noted in this study, the fusion of spatial and spectral information mainly benefited the physical characteristics more than the chemical properties. For angle flop, the RPD value for sole spectral information indicated very poor model,[43] while for sole spatial information, the model fall in poor category,[43] the higher RPD for fusion model of spatial and spectral information indicated a fair model which can be deployed for screening purposes.[43] For finger press scoring, the RPD for sole spatial and spectral information indicated a very poor model not useful in practise, while the fusion model with higher RPD indicates that model can be used in rough screening applications.[43]

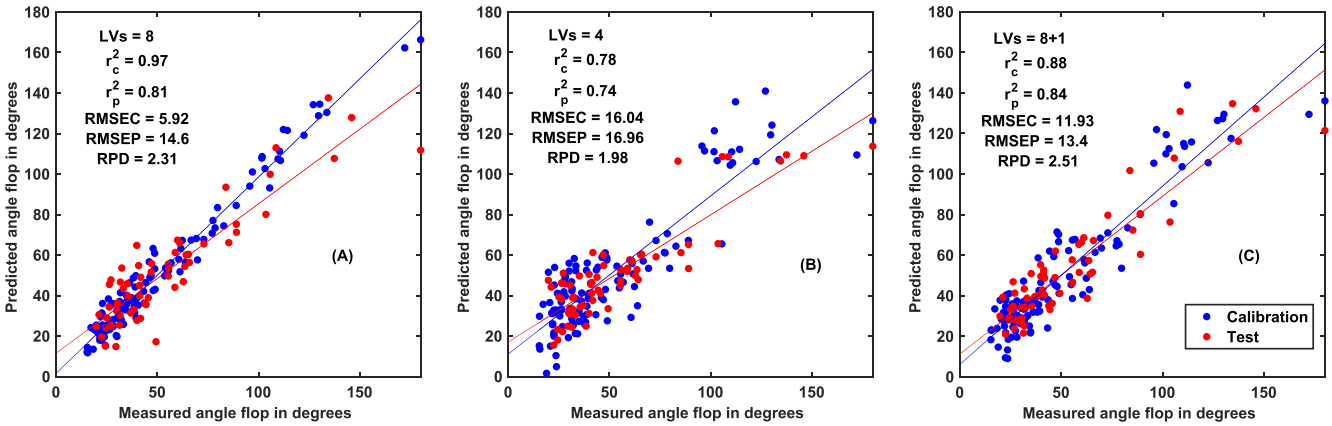

FIGURE 4 Angle flop prediction with (A) spatial information, (B) spectral information, and (C) sequential fusion model.

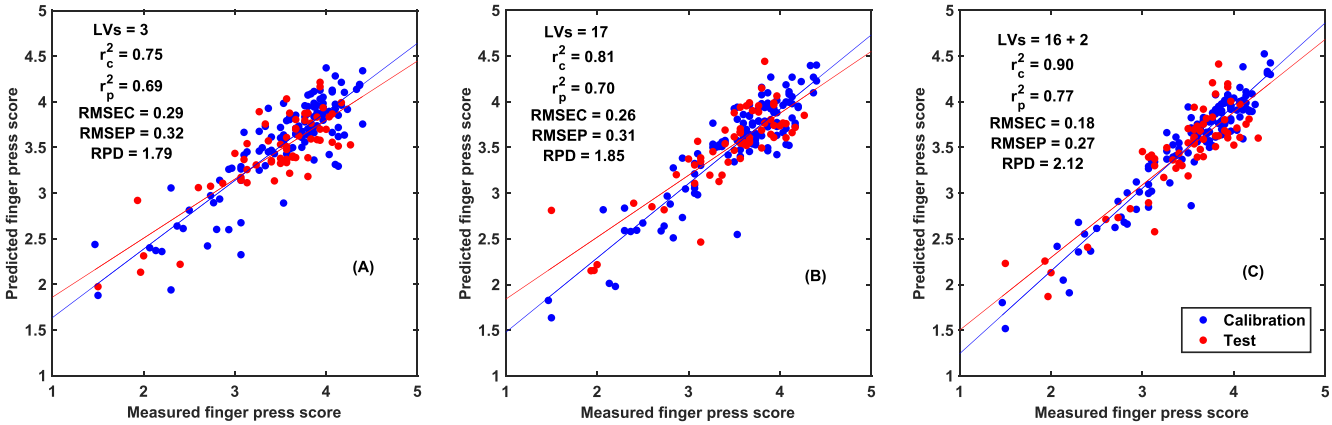

FIGURE 5 Finger press score prediction with (A) spatial information, (B) spectral information, and (C) sequential fusion model.

4 | DISCUSSION AND CONCLUSIONS

The study presented a novel approach to using both contextual spatial and spectral information for predictive modeling based on HSI. The deep features extracted by the ResNet-18 pretrained model were able to predict different physico-chemical properties. For chemical properties, the model based on spatial features performed poorer than the model based on spectral features in terms of RMSEP and RPD. For physical properties, the model based on spatial features performed better than spectral features. The fusion approach showed that it improved the model performance for predicting physical parameters, indicating that spatial and spectral information carry complementary information for predicting physical properties.

In some earlier studies, NIR spectroscopy has already been used for predicting several chemical properties such as iodine and FA compositions.[44,45] Earlier studies commonly used a spectral range of up to 2500 nm as clear peaks related to fat are present in such a range. This study utilized the spectral range only up to 1000 nm, which is mainly composed of a mixture of several bonds third overtones. The main reason for using such a range is the low cost of the spectral sensor compared with a spectral sensor operating up to the 2500 nm spectral range. RGB color imaging has also been used in the analysis of pork quality. For example,[46] used RGB imaging to detect PSE (pale, soft, exudative) defects in pork. Such analysis used the color lightness as an indicator of meat quality. In another study, RGB imaging has also been used for predicting intramuscular fat.[47] In this study, the deep features extracted with pseudo RGB images were able to explain the chemical properties as well but not as well as the spectral features. The RGB data were pseudo-generated from HSI data. A step to improve the results of RGB imaging could be to use a separate high-resolution RGB camera which can capture detailed features. The hyperspectral cameras currently available on the market usually have low spatial resolution.

The typical approach to hyperspectral image processing is either pixel-wise analysis using chemometric models[21] or based on image analysis using DL approaches.[17] Pixel-wise predictions are mainly performed when there is spatial heterogeneity and also interest in exploring the spatial differences in properties. In the presented results, we did not perform pixel-wise predictions to generate chemical maps. This is mainly because we were already extracting and imaging only the fat part of the carcass and were interested in the average value of predicted properties. If needed, for pixel-wise chemical map generation, instead of mean spectra, the user can simply use pixel spectra and generate chemical maps as well; there are no restrictions on that. To enhance the extraction of spatial information from the local pixel neighborhood, the user can feed the local region to the DL model for local spatial feature extraction.

The developed approach can be applied to every application of HSI where predictive models (classification/regression) need to be developed at the object level. The approach of feature extraction with DL is straightforward and does not require any training for the deep model. In fact, as DL models advance in the area of computer vision, it is expected that the feature extraction will become more refined as well. In some recent studies, older concepts such as grey level co-occurrence matrices[22,23] and wavelet transformation[48] were used for manual hyperspectral feature extraction; however, pretrained DL models (available open source) allow an automatic approach to extract deep multiscale features, thus also saving time and extra manual analysis.

In the current study, while observing the pseudo-RGB images with the naked eye (results not presented), it was difficult to see something visually different in RGB images which can be directly related to the explanation of the chemical and physical properties. It was assumed that with multiscale feature extraction using DL, minute details that are difficult to detect visually by the naked eye can be captured. In future research, the development of methods to explain the deep models is needed. Such model explanation will allow pinpointing the exact spatial location/features which carry relevant differences in samples.

ACKNOWLEDGMENTS

The authors would like to thank the researchers Begonya Marcos (IRTA) and Juan Florencio Tejeda (UEX) and the IRTA technicians Albert Brun, Agustí Quintana, Albert Rossell, Adrià Pacreu, Cristina Canals, and Joel González, for their help in the execution of the project. Thanks also given to José M. Martínez for their contribution in the analysis of fatty acids. The authors thank the Spanish National Institute of Agricultural Research (INIA) for the scholarship to Michela Albano-Gaglio (PRE2019-089669). This work was partly funded by the Spanish Ministry of Science and Innovation, project number RTI2018-096993-B-I00. The CERCA programme from the Generalitat de Catalunya is also acknowledged.

PEER REVIEW

The peer review history for this article is available at https://www.webofscience.com/api/gateway/wos/peer-review/10.1002/cem.3552.

ORCID

Puneet Mishra https://orcid.org/0000-0001-8895-798X

REFERENCES

1. Boldrini B, Kessler W, Rebner K, Kessler RW. Hyperspectral imaging: a review of best practice, performance and pitfalls for in-line and on-line applications. *J Near Infrared Spectrosc*. 2012;20(5):483-508.
2. Manley M. Near-infrared spectroscopy and hyperspectral imaging: non-destructive analysis of biological materials. *Chem Soc Rev*. 2014;43(24):8200-8214.
3. Lu Y, Saeys W, Kim M, Peng Y, Lu R. Hyperspectral imaging technology for quality and safety evaluation of horticultural products: a review and celebration of the past 20-year progress. *Postharvest Biol Technol*. 2020;170:111318.
4. Wieme J, Mollazade K, Malounas I, Zude-Sasse M, Zhao M, Gowen A, Argyropoulos D, Fountas S, Van Beek J. Application of hyperspectral imaging systems and artificial intelligence for quality assessment of fruit, vegetables and mushrooms: a review. *Biosyst Eng*. 2022;222:156-176.
5. Walsh KB, Blasco J, Zude-Sasse M, Sun X. Visible-NIR point spectroscopy in postharvest fruit and vegetable assessment: the science behind three decades of commercial use. *Postharvest Biol Technol*. 2020;168:111246.
6. Shi W, Koo DES, Kitano M, et al. Pre-processing visualization of hyperspectral fluorescent data with spectrally encoded enhanced representations. *Nature Commun*. 2020;11(1):726.
7. Al Ktash M, Stefanakis M, Englert T, et al. Uv hyperspectral imaging as process analytical tool for the characterization of oxide layers and copper states on direct bonded copper. *Sensors*. 2021;21(21):7332.
8. Kandpal LM, Lee S, Kim MS, Bae H, Cho B-K. Short wave infrared (SWIR) hyperspectral imaging technique for examination of aflatoxin B1 (AFB1) on corn kernels. *Food Control*. 2015;51:171-176.
9. E Brito LR, Chaves AB, Braz A, Pimentel MF. Raman hyperspectral imaging and a novel approach for objective determination of the order of crossing ink lines. *Spectrochim Acta Part A: Mol Biomol Spectrosc*. 2019;223:117287.
10. Bøtker J, Wu JX, Rantanen J. Hyperspectral imaging as a part of pharmaceutical product design. *Data Handling in Science and Technology*, Vol. 32: Elsevier; 2019:567-581.
11. Mishra P, Sytsma M, Chauhan A, Polder G, Pekkeriet E. All-in-one: a spectral imaging laboratory system for standardised automated image acquisition and real-time spectral model deployment. *Anal Chim Acta*. 2022;1190:339235.
12. Xiong Z, Xie A, Sun D-W, Zeng X-A, Liu D. Applications of hyperspectral imaging in chicken meat safety and quality detection and evaluation: a review. *Critical Rev Food Sci Nutrit*. 2015;55(9):1287-1301.
13. Jia W, van Ruth S, Scollan N, Koidis A. Hyperspectral imaging (HSI) for meat quality evaluation across the supply chain: current and future trends. *Current Res Food Sci*. 2022;5:1017-1027.
14. Zhuang Q, Peng Y, Yang D, Wang Y, Zhao R, Chao K, Guo Q. Detection of frozen pork freshness by fluorescence hyperspectral image. *J Food Eng*. 2022;316:110840.
15. Yu X, Tang L, Wu X, Lu H. Nondestructive freshness discriminating of shrimp using visible/near-infrared hyperspectral imaging technique and deep learning algorithm. *Food Anal Methods*. 2018;11:768-780.
16. Dixit Y, Reis MM. Hyperspectral imaging for assessment of total fat in salmon fillets: a comparison between benchtop and snapshot systems. *J Food Eng*. 2023;336:111212.
17. Mishra P. Deep generative neural networks for spectral image processing. *Anal Chim Acta*. 2022;1191:339308.
18. Saeys W, Do Trong NN, Van Beers R, Nicolaï BM. Multivariate calibration of spectroscopic sensors for postharvest quality evaluation: a review. *Postharvest Biol Technol*. 2019;158:110981.
19. Workman JJ. A review of calibration transfer practices and instrument differences in spectroscopy. *Appl Spectrosc*. 2018;72(3):340-365.
20. Wold S, Sjöström M, Eriksson L. Pls-regression: a basic tool of chemometrics. *Chemom Intell Lab Syst*. 2001;58(2):109-130.
21. Amigo JM, Babamoradi H, Elcoroaristizabal S. Hyperspectral image analysis. A tutorial. *Anal Chim Acta*. 2015;896:34-51.
22. Mishra P, Nordon A, Asaari MSM, Lian G, Redfern S. Fusing spectral and textural information in near-infrared hyperspectral imaging to improve green tea classification modelling. *J Food Eng*. 2019;249:40-47.
23. Gaci B, Abdelghafour F, Ryckewaert M, Mas-Garcia S, Louargant M, Verpont F, Laloum Y, Bendoula R, Chaix G, Roger J-M. A novel approach to combine spatial and spectral information from hyperspectral images. *Chemom Intell Lab Syst*. 2023;240:104897.
24. Herrero-Langreo A, Gorretta N, Tisseyre B, Gowen A, Xu J-L, Chaix G, Roger J-M. Using spatial information for evaluating the quality of prediction maps from hyperspectral images: a geostatistical approach. *Anal Chim Acta*. 2019;1077:116-128.
25. Chai J, Zeng H, Li A, Ngai EWT. Deep learning in computer vision: a critical review of emerging techniques and application scenarios. *Mach Learn Appl*. 2021;6:100134.
26. Zhao Z, Alzubaidi L, Zhang J, Duan Y, Gu Y. A comparison review of transfer learning and self-supervised learning: definitions, applications, advantages and limitations. *Expert Syst Appl*. 2023;2023:122807.
27. Mishra P, Passos D. Realizing transfer learning for updating deep learning models of spectral data to be used in new scenarios. *Chemom Intell Lab Syst*. 2021;212:104283.

28. Al-Areqi F, Konyar MZ. Effectiveness evaluation of different feature extraction methods for classification of Covid-19 from computed tomography images: a high accuracy classification study. *Biomed Signal Process Control*. 2022;76:103662.
29. Puls ES, Todescato MV, Carbonera JL. An evaluation of pre-trained models for feature extraction in image classification. arXiv preprint arXiv:231002037; 2023.
30. Mishra P, Roger J-M, Jouan-Rimbaud-Bouveresse D, Biancolillo A, Marini F, Nordon A, Rutledge DN. Recent trends in multi-block data analysis in chemometrics for multi-source data integration. *TrAC Trends Anal Chem*. 2021;137:116206.
31. Naes T, Tomic O, Afseth NK, Segtnan V, Måge I. Multi-block regression based on combinations of orthogonalisation, pls-regression and canonical correlation analysis. *Chemom Intell Lab Syst*. 2013;124:32-42.
32. Orth SH, Marini F, Fox GP, Manley M, Hayward S. Multiblock spectral imaging for identification of pre-harvest sprouting in hordeum vulgare. *Microchem J*. 2023;191:108742.
33. Mishra P, Xu J. Multimodal close range hyperspectral imaging combined with multiblock sequential predictive modelling for fresh produce analysis. *J Near Infrared Spectrosc*. 2023;31(3):141-149.
34. AOAC. The association of official analytical chemists international. *Official Methods Anal*. 2000;38(8).
35. Bligh EG, Dyer WJ. A rapid method of total lipid extraction and purification. *Canadian J Biochem Physiol*. 1959;37(8):911-917.
36. Front matter. In: Sandler SR, Karo W, eds. *Sourcebook of Advanced Organic Laboratory Preparations*. Boston: Academic Press; 1992:iii. https://www.sciencedirect.com/science/article/pii/B9780080925530500017
37. Fiego DPL, Minelli G, Volpelli LA, Ulrici A, Macchioni P. Calculating the iodine value for italian heavy pig subcutaneous adipose tissue from fatty acid methyl ester profiles. *Meat Sci*. 2016;122:132-138.
38. Thiel-Cooper RL, Parrish Jr FC, Sparks JC, Wiegand BR, Ewan RC. Conjugated linoleic acid changes swine performance and carcass composition. *J Animal Sci*. 2001;79(7):1821-1828.
39. Soladoye OP, Uttaro B, Zawadski S, Dugan MER, Gariépy C, Aalhus JL, Shand P, Juárez M. Compositional and dimensional factors influencing pork belly firmness. *Meat Sci*. 2017;129:54-61.
40. Kennard RW, Stone LA. Computer aided design of experiments. *Technometrics*. 1969;11(1):137-148.
41. Rabatel G, Marini F, Walczak B, Roger J-M. VSN: variable sorting for normalization. *J Chemom*. 2020;34(2):e3164.
42. He K, Zhang X, Ren S, Sun J. Deep residual learning for image recognition. In: Proceedings of the IEEE Conference on Computer Vision and Pattern Recognition; 2016:770-778.
43. Williams P. The RPD statistic: a tutorial note. *NIR News*. 2014;25(1):22-26.
44. Foca G, Ferrari C, Ulrici A, Ielo MC, Minelli G, Lo Fiego DP. Iodine value and fatty acids determination on pig fat samples by FT-NIR spectroscopy: benefits of variable selection in the perspective of industrial applications. *Food Anal Methods*. 2016;9:2791-2806.
45. Prieto N, Dugan MER, Juárez M, López-Campos O, Zijlstra RT, Aalhus JL. Using portable near-infrared spectroscopy to predict pig subcutaneous fat composition and iodine value. *Canadian J Animal Sci*. 2017;98(2):221-229.
46. Chmiel M, Słowiński M, Dasiewicz K. Lightness of the color measured by computer image analysis as a factor for assessing the quality of pork meat. *Meat Sci*. 2011;88(3):566-570.
47. Faucitano L, Huff P, Teuscher F, Gariepy C, Wegner J. Application of computer image analysis to measure pork marbling characteristics. *Meat Sci*. 2005;69(3):537-543.
48. Ahmad M, Vitale R, Silva CS, Ruckebusch C, Cocchi M. Exploring local spatial features in hyperspectral images. *J Chemom*. 2020; 34(10):e3295.

How to cite this article: Mishra P, Albano-Gaglio M, Font-i-Furnols M. A short note on deep contextual spatial and spectral information fusion for hyperspectral image processing: Case of pork belly properties prediction. *Journal of Chemometrics*. 2024;e3552. doi:10.1002/cem.3552